Supporting Information for

Control of Ice Formation

*Ching-Wen Lo, Venkataraman Sahoo, and Ming-Chang Lu**

Department of Mechanical Engineering, National Chiao Tung University, Hsinchu, Taiwan 300

Corresponding Authors: *E-mail: mclu@mail.nctu.edu.tw

Table S1. Water contact angles on different surfaces

Name	θ^a [°]	$\theta_{adv}{}^a$ [°]	$\theta_{rec}{}^a$ [°]	$\theta_{CAH}{}^a$ [°]
Plain Si	100 ± 2	115 ± 2	35 ± 1	~80
SiNW	150 ± 4	151 ± 2	147 ± 2	<5
TMG-125	140 ± 2	145 ± 1	85 ± 2	~60
VMG-125	140 ± 1	145 ± 2	85 ± 4	~60
VMG-165	142 ± 2	145 ± 2	85 ± 4	~60
VMG-250	142 ± 2	146 ± 2	86 ± 4	~60

[a] θ, θ_{adv}, θ_{rec}, and θ_{CAH} are equilibrium contact angle, advancing contact angle, receding contact angle, and contact angle hysteresis, respectively.

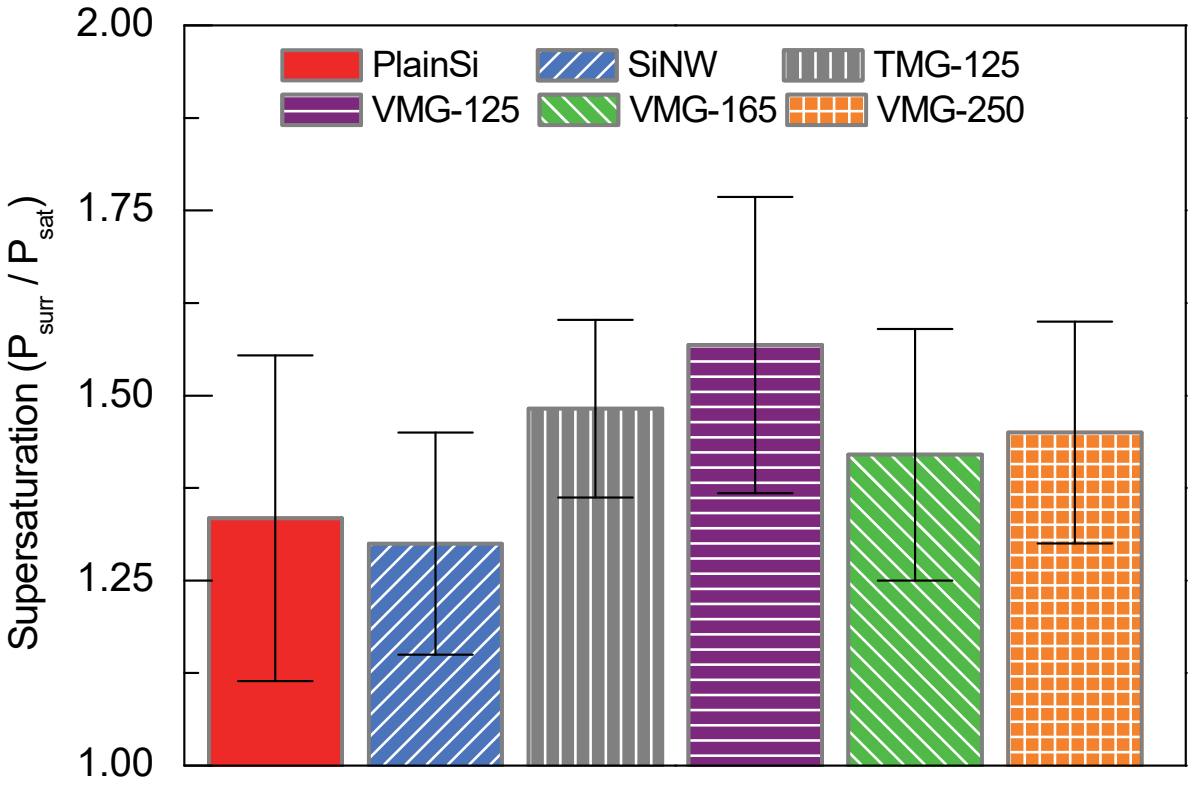

Figure S1. Threshold supersaturations for ice nucleation on the surfaces. The threshold supersaturation for ice nucleation was recorded when initial ice embryo is observed on the surfaces in the ESEM. The threshold supersaturations for initial ice nucleation on the surfaces are between 1.1 and 1.76. We found that the relationship between surface structure and threshold of supersaturation for ice nucleation was not definite presumably due to the large uncertainties. The error bars in the figure represent the standard deviation.

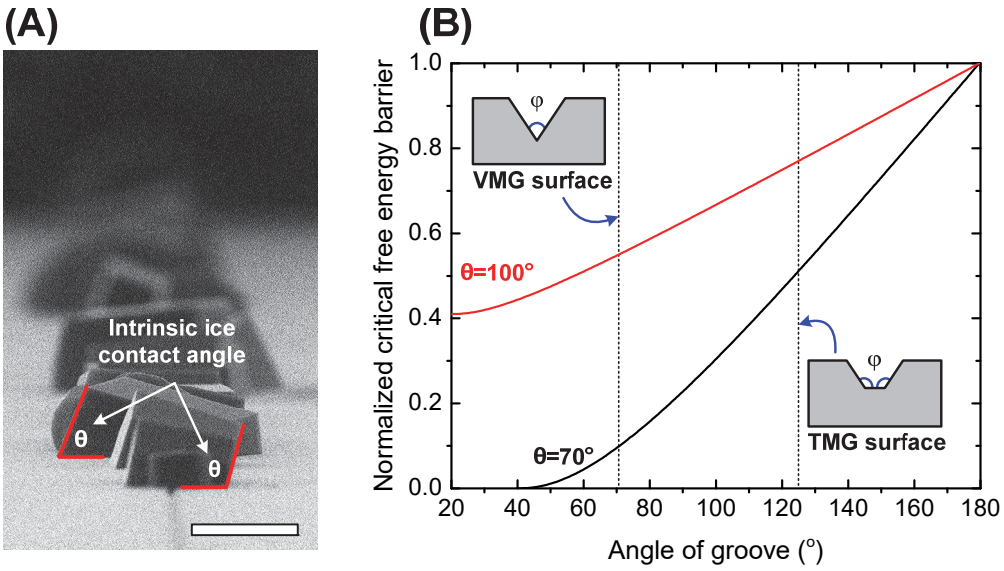

Figure S2. The normalized critical free energy barrier. (A) The intrinsic ice contact angle on the TMG-125 surface. The supersaturation is ~ 1.2, and the scale bar is 50 μm. (B) The ϕ dependent normalized critical free energy barrier for ice crystal nucleation on the grooved surfaces.

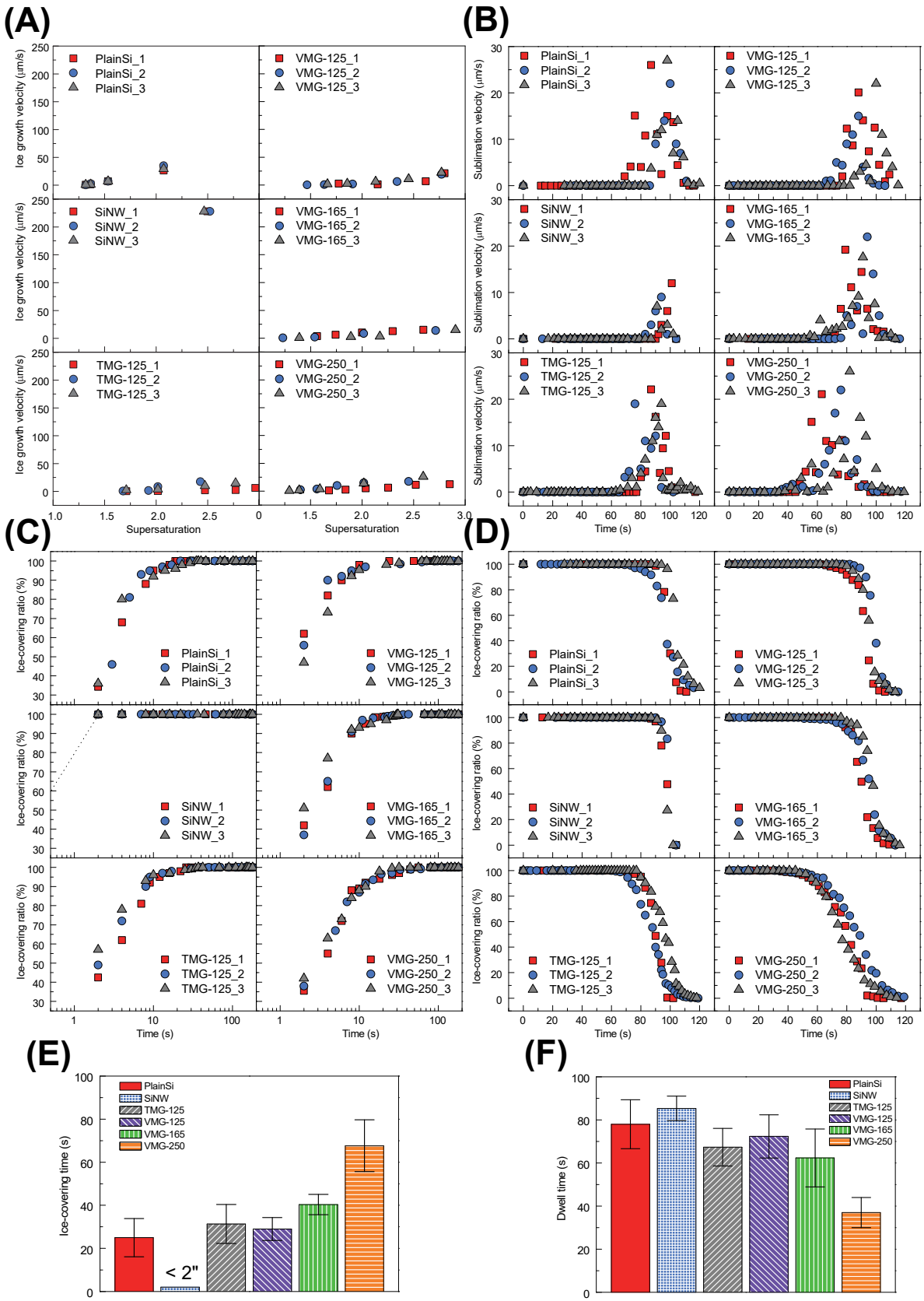

Figure S3. The whole set of the experimental results in icing and deicing experiments. Three repeated experiments were conducted on the surfaces. The three symbols in each panel in

Figure S3A−D represent the results from the three repeated measurements on a surface, respectively. Figure S3 includes one set of data which was already presented in the main text. The errors in Figure S3E,F are the standard deviation. The six panels in Figure S3A−D depict the experimental data obtained on the six different surfaces, respectively (*i.e.*, plain Si, SiNW, TMG-125, VMG-125, VMG-165, and VMG-250). (A,B) The ice growth velocity and sublimation velocity on the surfaces, respectively. (C,D) The ice-covering ratio during the icing and deicing experiments, respectively. (E,F) Ice-covering times and dwell times on the surfaces, respectively. Note that ice-covering time on the SiNW surface was too short (< 2 sec) to be determined in the ESEM.

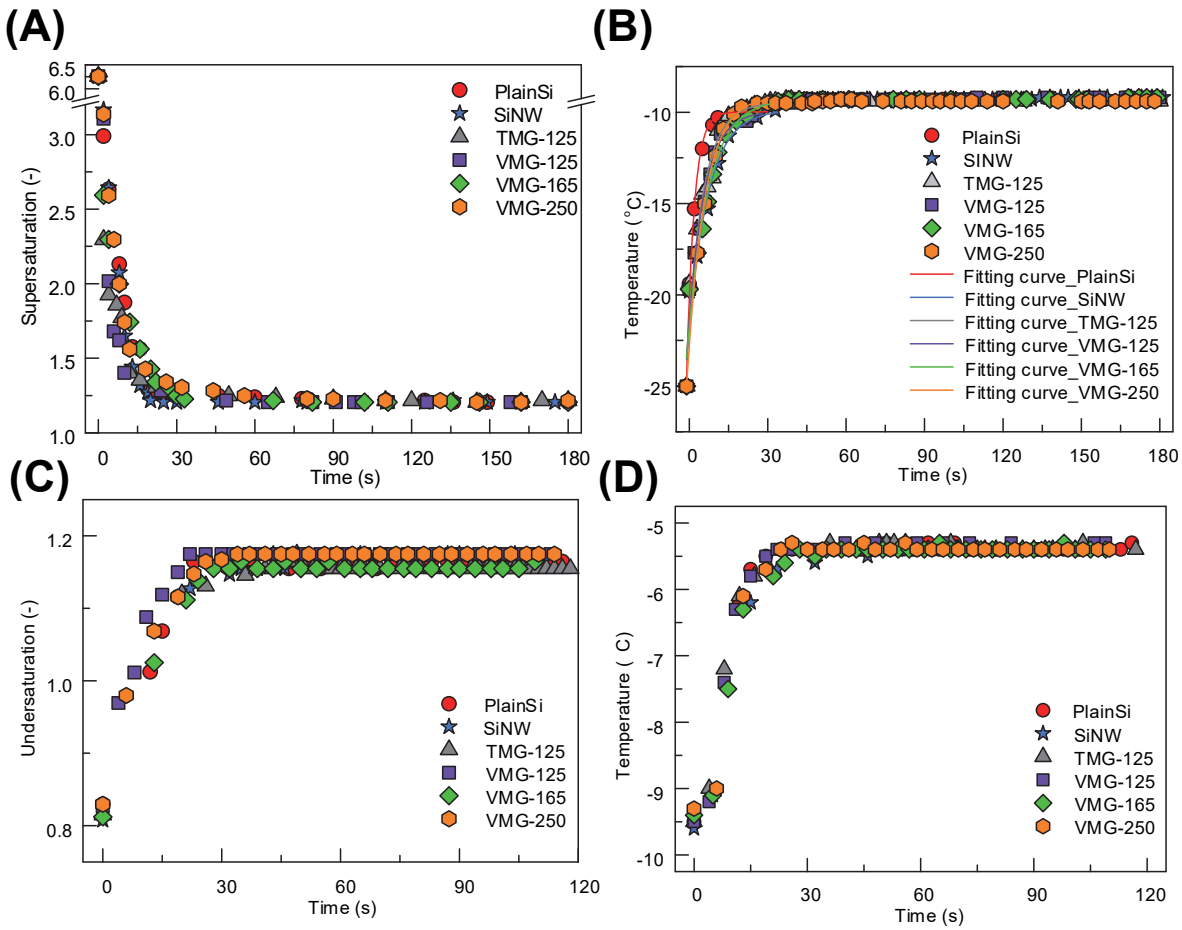

Figure S4. Variations of supersaturation, undersaturation, and surface temperature. (A,B) supersaturation and surface temperature as a function of time during the icing experiments, respectively. (C,D) Undersaturation and surface temperature as a function of time during deicing experiments, respectively.

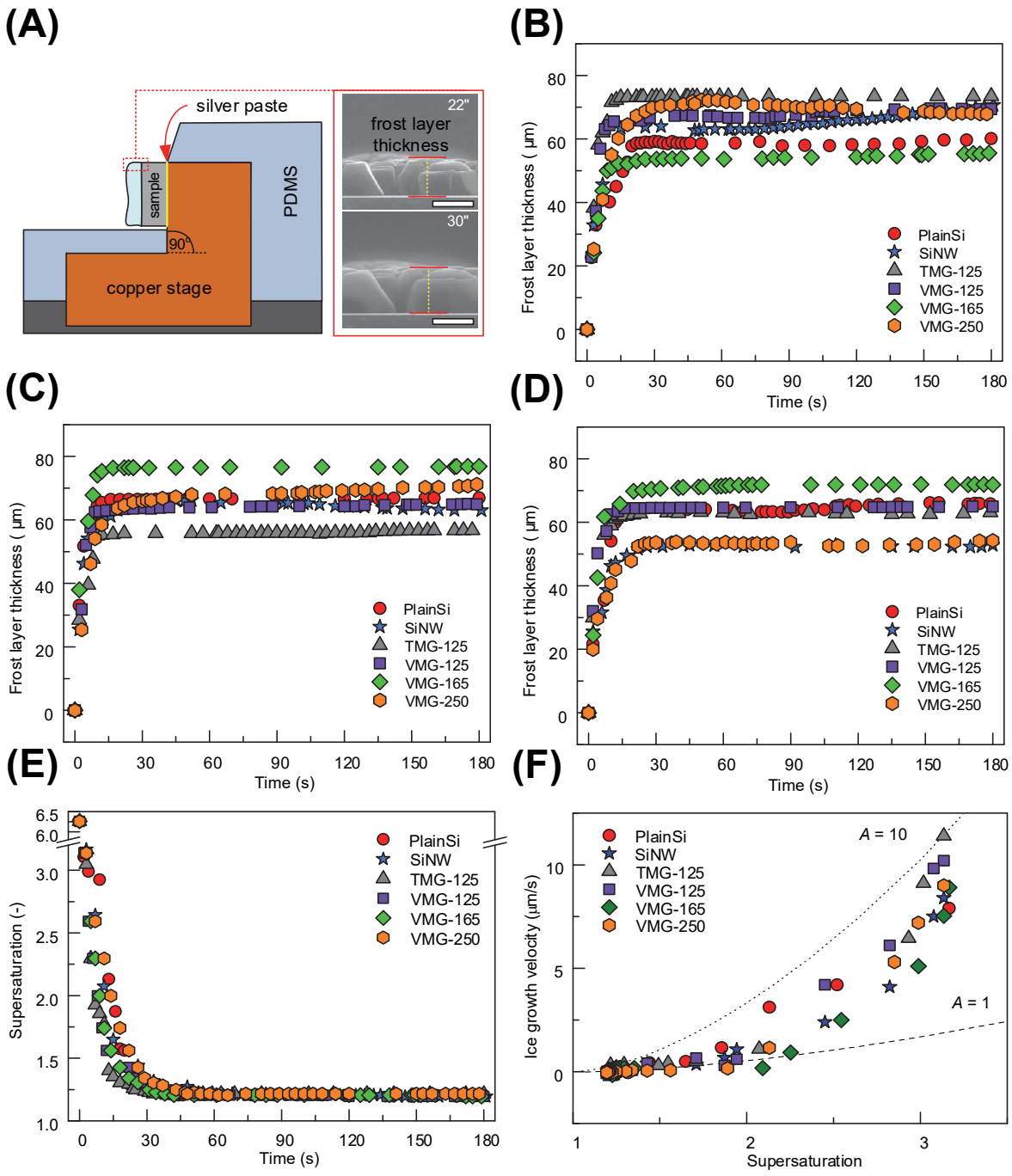

Figure S5. Thickness of ice layer. (A) The schematic of the 90° tilted stage for characterizing the cross-sectional ice thickness in the ESEM. The scale bars in ESEM images are 50 μm and the schematic is not in real scale. The measured cross-sectional ice thicknesses as a function of time on the studied surfaces obtained from three repeated experiments are shown in (B), (C), and (D), respectively. (E) Supersaturation as a function of time. (F) The corresponding vertical ice growth velocity as a function of

supersaturation (data obtained from Figure S5B). The solid symbols and lines are the measured velocities and the theoretical predictions of Equation (3) with different A, respectively.

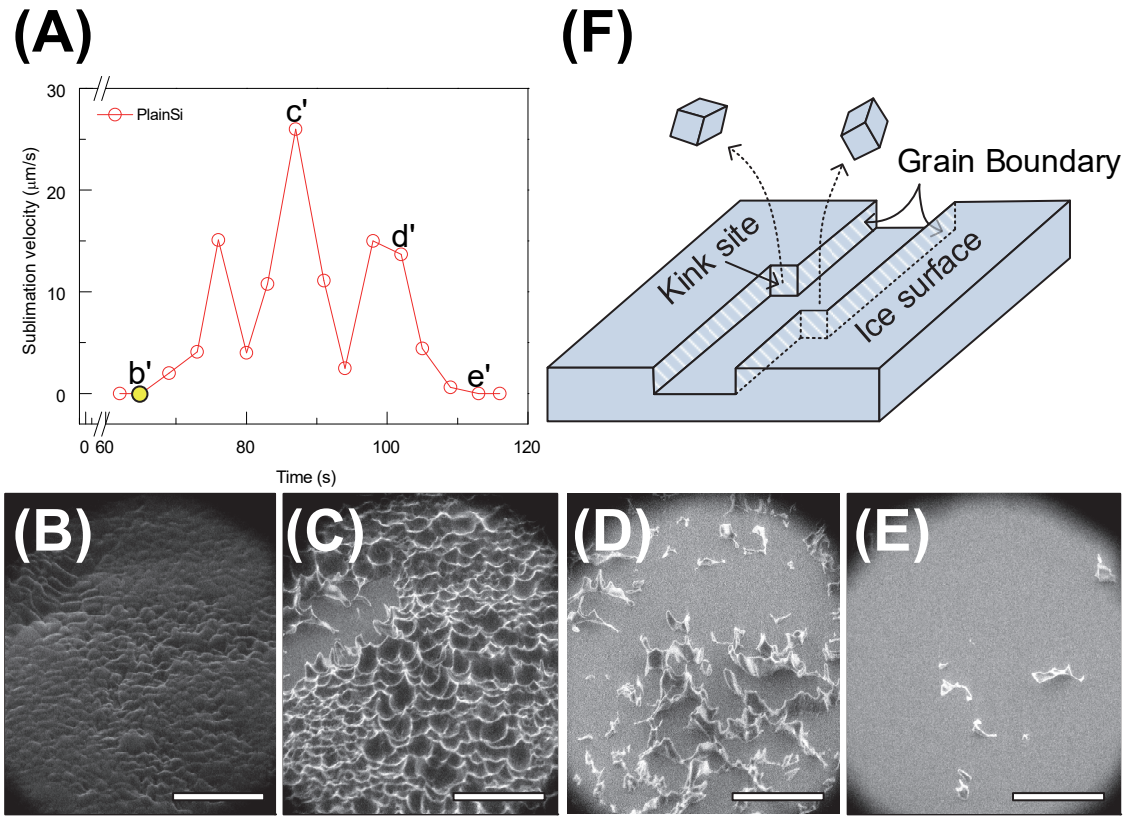

Figure S6. Quantitative analysis of the sublimation velocity on the plain Si surface. (A) The measured sublimation velocity during the deicing process on the plain Si surface. (B), (C), (D), and (E) are the corresponding topographies on the ice surface at the points b′, c′, d′ and e′ in Figure S6A. (F) The grain boundary could provide kink sites. Scale bars are in 200 μm.

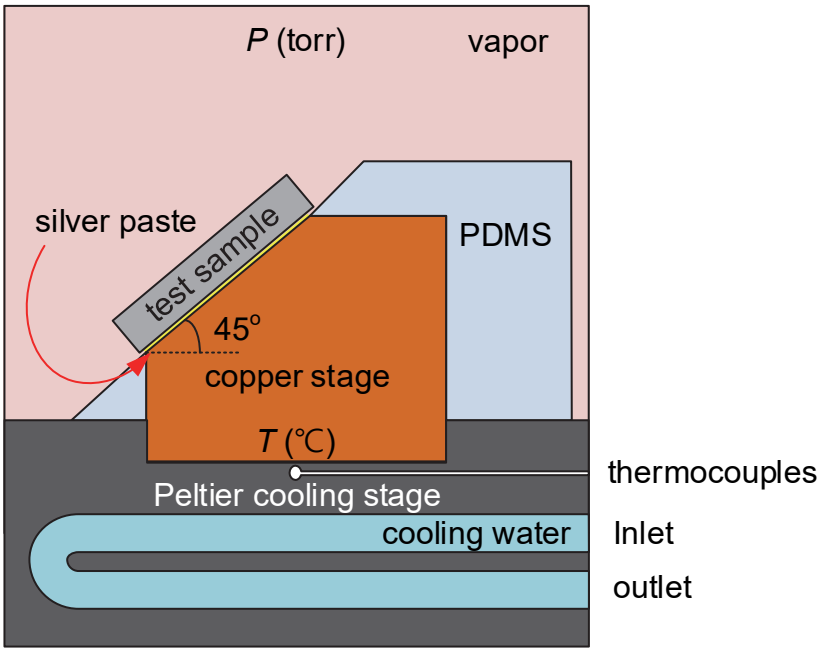

Figure S7. Test section for conducting frosting and deicing experiments in the ESEM chamber.

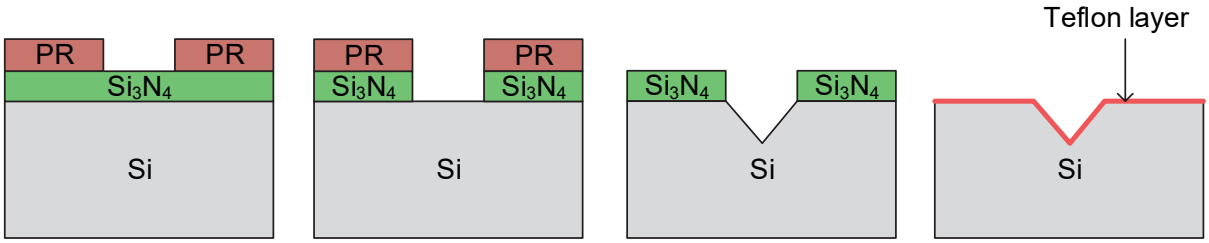

Figure S8. Fabrication procedure of the microgroove superhydrophobic surfaces.

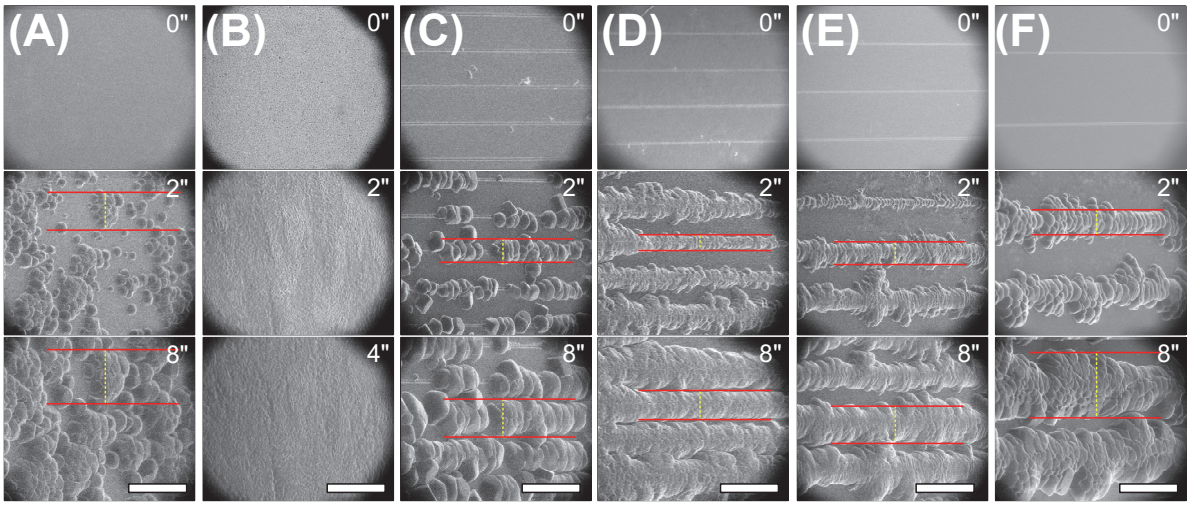

Figure S9. The methods for determining ice growth velocity during icing experiments. Selected snapshots of ice-covering evolution during icing on (A) plain Si, (B) SiNW, (C) TMG-125, (D) VMG-125, (E) VMG-165 and (F) VMG-250 surfaces. Red solid line and yellow dash line represent the wavefront and characteristic length of the ice crystal, respectively. Scale bars are in 200 μm.

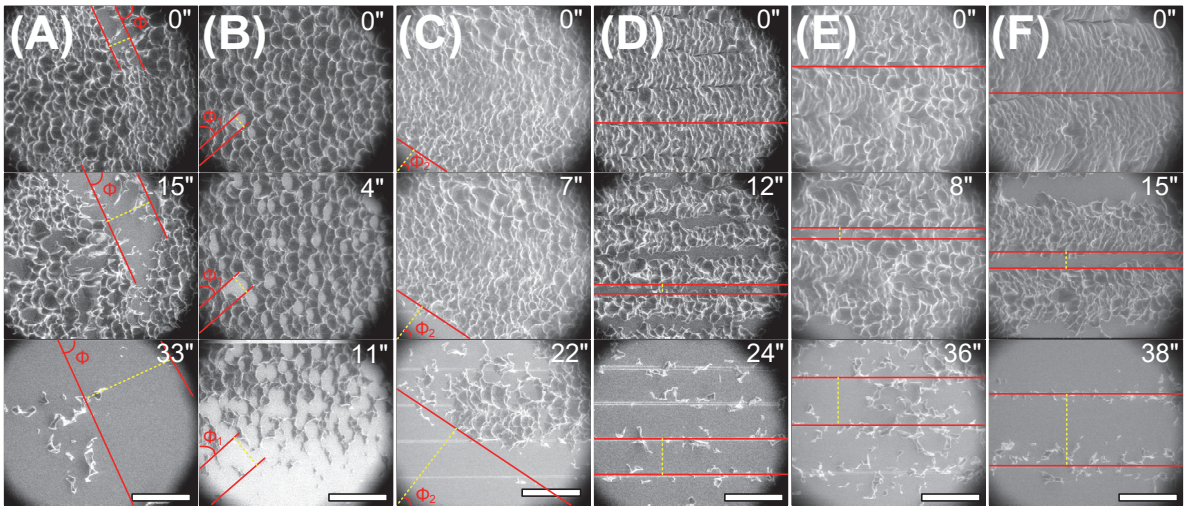

Figure S10. The methods for determining the sublimation velocity in the deicing processes. Selected snapshots of deicing processes on (A) plain Si, (B) SiNW (C) TMG-125, (D) VMG-125, (E) VMG-165 and (F) VMG-250 surfaces. Red solid line and yellow dash line represent the wavefronts and the length between the wavefronts, respectively. Φ, Φ_1, and Φ_2 are the angles for defining receding wavefronts on the plain Si, SiNW and TMG surfaces. Scale bars in the figures are 200 μm.